OPTOELECTRONICS AND ADVANCED MATERIALS – RAPID COMMUNICATIONS Vol. 15, No. 11-12, November-December 2021, p. 624-631

Spatial distribution of structural and morphological features of few layered intercalated graphene

BALAJI CHANDRA[a], MATHEW K. FRANCIS[a], P. BALAJI BHARGAV[a,*], NAFIS AHMED[a], SWAYAM KESARI[b], REKHA RAO[b], ADITHYA JOSEPH ANTONYSAMY[c]
[a]*SSN Research Centre, Sri Sivasubramaniya Nadar College of Engineering, Kalavakkam, Tamilnadu 603110, India*
[b]*Solid State Physics Division, Bhabha Atomic Research Centre, Mumbai-400085, India*
[c]*Department of Civil and Environmental Engineering, Stanford University, California 94305, USA*

Few layered graphene (FLG) is grown using chemical vapor deposition (CVD) technique using copper (Cu) as a catalyst. Structural and morphological features of graphene layers grown for different time periods are examined using maps of various Raman intensity ratios, X-ray photoemission spectroscopy (XPS) spectrum and field emission scanning electron microscopy (FESEM) images. Average distance between defects in the grown graphene is calculated to range from 28 nm to 19 nm. Oxygen to carbon ratio in the grown graphene is estimated to be 0.18. Properties of FLG intercalated with $FeCl_3$ are also studied.

(Received March 31, 2021; accepted November 24, 2021)

Keywords: Graphene, CVD, Intercalation, Raman spectroscopy, FESEM, XPS

1. Introduction

Among the various allotropes of carbon graphene, a sp^2 allotrope, has gained widespread attention since its discovery owing to its potential applications [1]. Graphene was first isolated from graphite flakes using micromechanical cleavage [2]. Since then, many techniques have been developed for the synthesis of graphene [3]. Chemical vapour deposition (CVD) is one among the many graphene synthesis techniques. CVD growth of graphene has various advantages, when compared to other growth techniques, such as: process controllability, scalability and relatively defect free synthesis [3]. One of the key parameters, in the CVD process, used to control the growth of graphene is the growth time. By controlling the growth time, one could control the evolution of the graphene layer over the catalyst substrate used [4]. An effort is made in this work to study the effect of growth time on the growth of graphene using various characterization techniques such as Raman spectroscopy, FESEM imaging and XPS. FESEM has emerged as an effective technique to image the morphologies of graphene. It can detect impurities, ruptures, folds and voids in graphene synthesized and transferred to various substrates in a quick and non-invasive manner [5]. In this study, graphene synthesized on Cu foils are investigated using FESEM. Raman spectroscopy is a versatile tool to study the properties of graphene. It can be used to study graphene synthesized by any method and on any substrate [6,7]. A variety of information about the synthesized graphene such as number of layers, type of stacking, structural deformations and chemical modifications introduced is provided by Raman spectroscopy [8]. Disorders and symmetry breaking defects are usually present in CVD synthesized graphene. Their presence and characteristics can be analyzed using Raman spectroscopy [9]. Average distance between the defects (L_D) is one measure of disorder present in graphene which can be calculated using information obtained from the Raman spectrum [9]. L_D corresponding to various FLGs synthesized in this work are calculated. Graphene layers can stack on top of each other. In stacks, two consecutive layers are oriented in such a way that one of the two sublattices of graphene aligns directly above one of the sublattices of the other layer. Based on where the second set of atoms (or) the second sublattice of graphene is placed, stacking order is determined. When the second sublattice atoms are placed above the center of the empty space of the hexagonal structure of graphene below, the stacking order is called AB Bernal stacking (Fig. 1(c)). In Bernal stacking, the hexagonal edges of consecutive layers are aligned in the same direction. While in the case of turbostatic stacking, the edges are rotated by 30° [10]. The stacking order can be determined using intensity ratios extracted from Raman spectrum [10]. Maps of Raman features are used to comment about the stacking order of FLG synthesized in this work. X-ray photoelectron spectroscopy (XPS) is a surface sensitive technique used to analyze the chemical composition of the material of interest's surface and the various bonds contained in it. During XPS analysis the sample is irradiated with an X-ray beam while the number of electrons that escape and their kinetic energy are measured. This helps in quantifying the elemental composition and the nature of the chemical bonds [11]. The elemental composition of FLG synthesized in this study are analyzed using XPS. Intercalation is a process where molecules or atoms can enter at the edges of the domains of few layered graphene (FLG) structures and then diffuse to form a continuous layer between graphene

sheets (Fig. 1(b)) [12]. Because of the adsorption induced nature of doping introduced by the intercalation process, the Fermi level of graphene is modified without the introduction of impurities that substitute the carbon atoms in the graphene structure [13]. Metal chlorides are suitable candidates for intercalation as they make the process simple. Metal chlorides exhibit negative Gibbs free energy. Because of this the metal ions with positive charge in these metal chlorides readily gets reduced to metal ions with zero charge after accepting electrons from other materials [13]. Intercalation of graphene with molecules such as $FeCl_3$ is known to increase the charge carrier concentration and hence the Fermi energy of FLG. This increase in charge carriers populates the higher energy states with charge carriers leading to higher number of conducting states and thereby to higher conductivity [12]. Such highly conductive transparent graphene layers possess great potential as electrodes. Graphene grown using CVD process is intercalated using $FeCl_3$ and analysed using Raman spectroscopy.

2. Experimental

2.1. Graphene synthesis using CVD

Copper (Cu) foils of 25 µm thickness, 99.8% (metal basis) purchased from Alfa Aesar were used as a catalyst for the growth of graphene. The Cu substrates were pretreated in a solution of 5% (wt. %) HNO_3 diluted in deionized (DI) water to remove surface impurities. CVD growth chamber, made of quartz tube, was evacuated to 10^{-6} mbar pressure after loading the Cu foils into the chamber. A tubular furnace was used to raise the temperature of the growth chamber to 1020°C. Once the set temperature is reached, the Cu foils were treated with H_2 to enlarge the grain size. Following this treatment, precursor gases H_2 and CH_4, in the ratio 1:2, were introduced into the growth chamber. This flow was maintained for four different periods viz: 1, 5, 15 and 30 minutes. After the end of the stipulated growth time, the precursor gas supply was switched off and the growth chamber was cooled.

2.2. Transfer of graphene

Graphene synthesized on Cu foil was transferred on to SiO_2 substrate for characterization and intercalation using a polymethyl methacrylate (PMMA) assisted technique. PMMA solution containing 3.5% (wt. %) PMMA in Anisole was prepared. PMMA solution was then coated on the Cu\Gr stack using spin coating. A 0.1M ammonium persulfate ($(NH_4)_2S_2O_8$) was used to etch the copper foil. After 4 hours, the copper was etched leaving the Gr\PMMA stack floating on the etchant solution. The floating Gr\PMMA stack was carefully rinsed multiple times in DI water. Following the rinsing, the Gr\PMMA stack was fished on to SiO_2 substrate. Water droplets stuck between the SiO_2 substrate and Gr\PMMA were carefully removed by blowing nitrogen (N_2) gas. Finally, the PMMA layer was removed by treating the SiO_2\Gr\PMMA stack with acetone.

2.3. Intercalation of graphene

Graphene transferred on to SiO_2 was intercalated using $FeCl_3$. SiO_2\Gr stack was loaded into a tubular intercalation chamber made of quartz. 0.1 gm of $FeCl_3$ was loaded on a boat and placed inside the chamber. The SiO_2\Gr stack was placed downstream of $FeCl_3$. The intercalation chamber was heated using a two-zone furnace (Fig. 1(a)). The boat containing $FeCl_3$ was heated to approximately 320° C while the SiO_2\Gr stack was heated to approximately 350° C. Intercalation was carried out for 6 hours during which a steady flow of argon (Ar) gas was maintained inside the chamber.

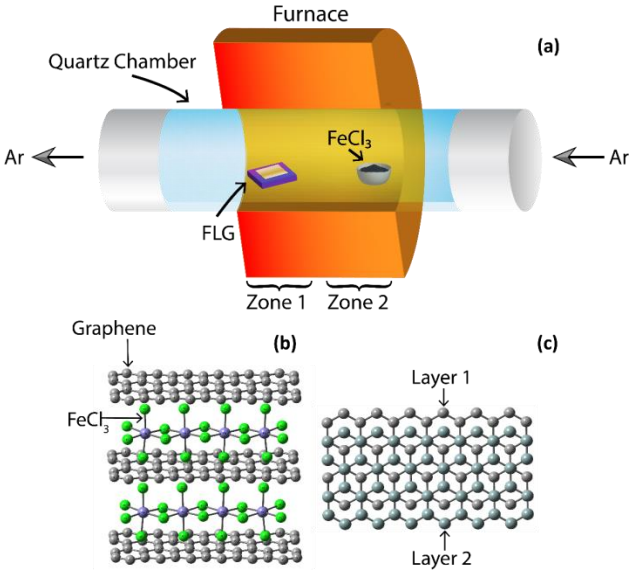

Fig. 1(a) Illustration of the two zone CVD furnace. (b) Illustration of FLG intercalated with $FeCl_3$. (c) Illustration of AB Bernal stacking of grapheme layers (color online)

2.4. Characterization

Raman spectroscopic studies were carried out using a Horiba-Jobin Yvon HR-800 Evolution instrument using 532 nm laser source and grating of 600 lines/mm. Raman spectroscopic data were analyzed by fitting the peaks to Lorentzians. Field emission scanning electron microscopy (FESEM) images of Cu\Gr stack were obtained using a JEOL, JSM-7001F microscope employing mixed mode - secondary electron (SE) and back scattered electron (BSE) – imaging. X-ray Photoemission Spectroscopy (XPS) spectrum of graphene transferred on to SiO_2 substrate was obtained using a Thermo Fischer Scientific ESCALAB Xi+ instrument using Al k alpha source with energy of 1486 eV.

3. Results and discussions

3.1. Morphology analysis

Imaging graphene using FESEM is challenging because the ultra-thin graphene layers are transparent to high energy electron beams and most often the morphology of the substrate beneath is imaged. By using low beam voltage (≤ 3Kv) one can ensure small beam/specimen interaction volume and thereby observe morphological features of grapheme [14]. Fig. 2(a) and (b) shows FESEM images of graphene with growth time corresponding to 1 minute and 5 minutes respectively. The insets show histogram of the marked areas in the FESEM image. Gray scale pixel values of a FESEM image are proportional to the received secondary electron intensity [14]. It is also known that the yield of back scattered electrons (BSE), received at the detector, are proportional to the atomic number of the molecule that the incident electrons interact with [14]. The mean grayscale value of the marked area in the FESEM image of graphene on Cu foil in Fig. 2(a) is approximately 73 and in Fig. 2(b) is approximately 189. The marked area in Fig. 2(a) corresponds to that of the copper substrate. It appears dark because oxidized copper has low atomic number and hence the BSE yield from it is lower [14]. It is well known that polycrystalline copper foil used to grow graphene is subject to oxidation from atmospheric agents and from diffusion of oxygen present in the Cu bulk towards the surface [14]. The marked area in Fig. 2(b) indicates higher yield of secondary electron (SE) and BSE collected by the detector, which can be attributed to graphene [14]. Even after careful treatment of copper foil some metallic impurities do remain on the foil after graphene growth process. Such impurities exhibit strong electron scattering thereby appearing as bright spots on FESEM image [15] as exhibited in Fig. 2(c).

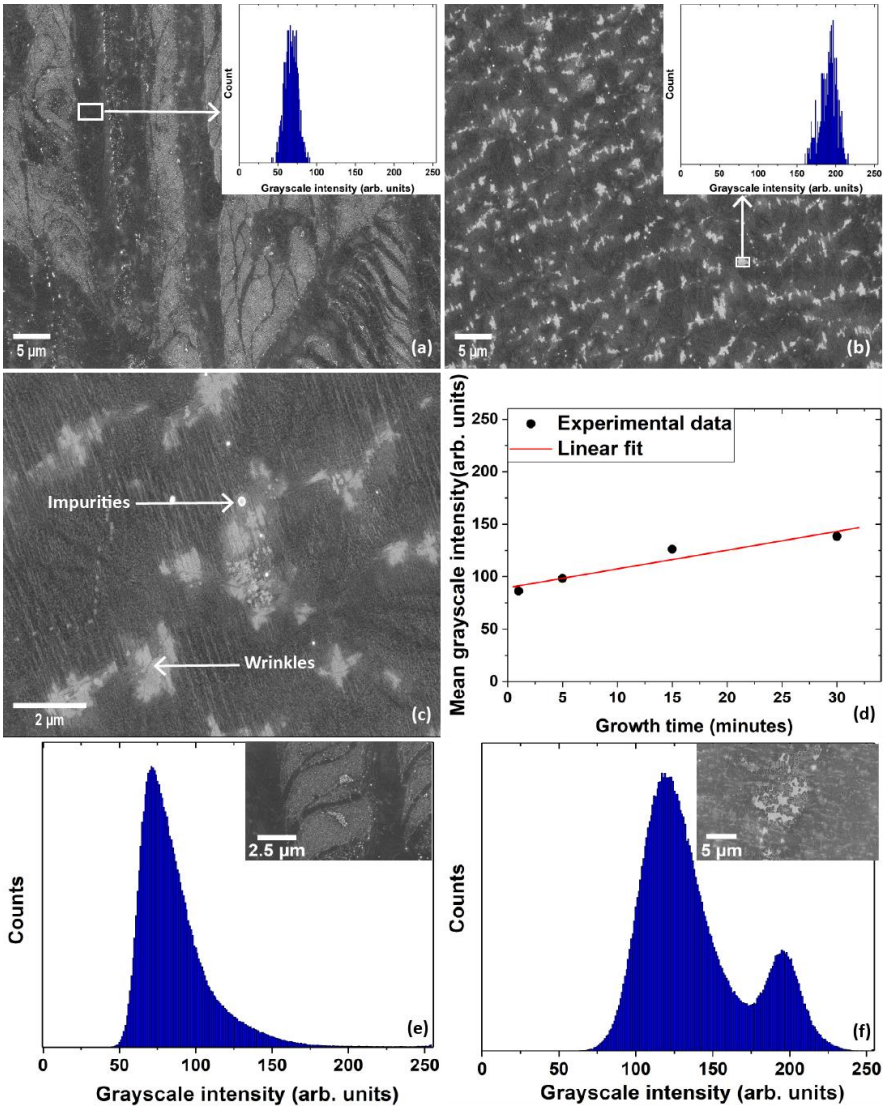

Fig. 2. FESEM image of graphene grown on Cu foil for 1 minute (a) and 5 minute (b), inset shows histogram of grayscale values of the marked area. (c) Impurities and wrinkles observed over Cu\Gr stack. (d) Graph plotting mean grayscale values of FESEM images of graphene grown on Cu foil for growth times of 1, 5, 15 and 30 minutes. Histogram of grayscale values of graphene grown for 1 min (e) and 30 min (f), insets show the corresponding grayscale images (color online)

Typical growth mechanism of graphene on Cu foil involves four stages: (1) incubation, (2) nucleation and growth (3) growth and coalescence (4) formation of films [4]. It has been shown that as the growth time increases, growth of graphene progresses along the four stages mentioned above [4]. Fig. 2 (e) &(f) depicts the evolution of the growth process through the histogram of the grayscale values of the FESEM images of graphene grown on Cu foil. The mean grayscale value of the imaged area, shown in the inset of Fig. 2(e), is approximately 86 indicating that majority of the imaged area constitutes copper foil. As the growth time increases the mean grayscale value increases reaching approximately 139 (Fig. 2(f)). The linear increase in mean grayscale values is plotted in Fig. 2(d). This indicates that a film of non-uniform, multilayer graphene, as confirmed by Raman analysis later, has grown on the Cu foil.

3.2. Raman spectroscopy analysis

Fig. 3(a) shows the Raman spectra of graphene grown using the CVD process employing different growth time viz. 1 min, 5 min, 15 min and 30 min. The spectra were obtained after transferring the grown graphene on to a SiO_2 substrate as described in the experimental section. Five peaks corresponding to frequencies around 1380, 1545, 1595, 1620 & 2690 cm^{-1} are evident in Fig. 3(a). The G band (1580 cm^{-1}) of graphene is associated with the doubly degenerate in-plane transverse optical (iTO) and longitudinal optical (LO) phonon modes (E_{2g} symmetry) at the Brillion zone [16]. This band occurs as a result of normal first order Raman scattering process. The 2D band (2690 cm^{-1}) originates from a second order Raman scattering process involving two iTO phonons near the K point [8]. Fig. 3(b) shows the deconvoluted Raman spectrum of the sample with growth time of 5 minutes. It is apparent that the G peak has split into two G^+(~1592 cm^{-1}) and G^-(1543 cm^{-1}). This splitting occurs when sp^2 carbon atoms gets deformed by rolling[17]. Rolled graphene induces polarization of Raman modes along the axis of the roll are called the longitudinal mode and along the curvature's circumference are called the tangential mode. The G^+ peak is attributed to the longitudinal mode and G^- peak is attributed to the tangential mode[17]. A 3-D visualization of folded graphene sheets is shown in Fig. 3(d) [18].

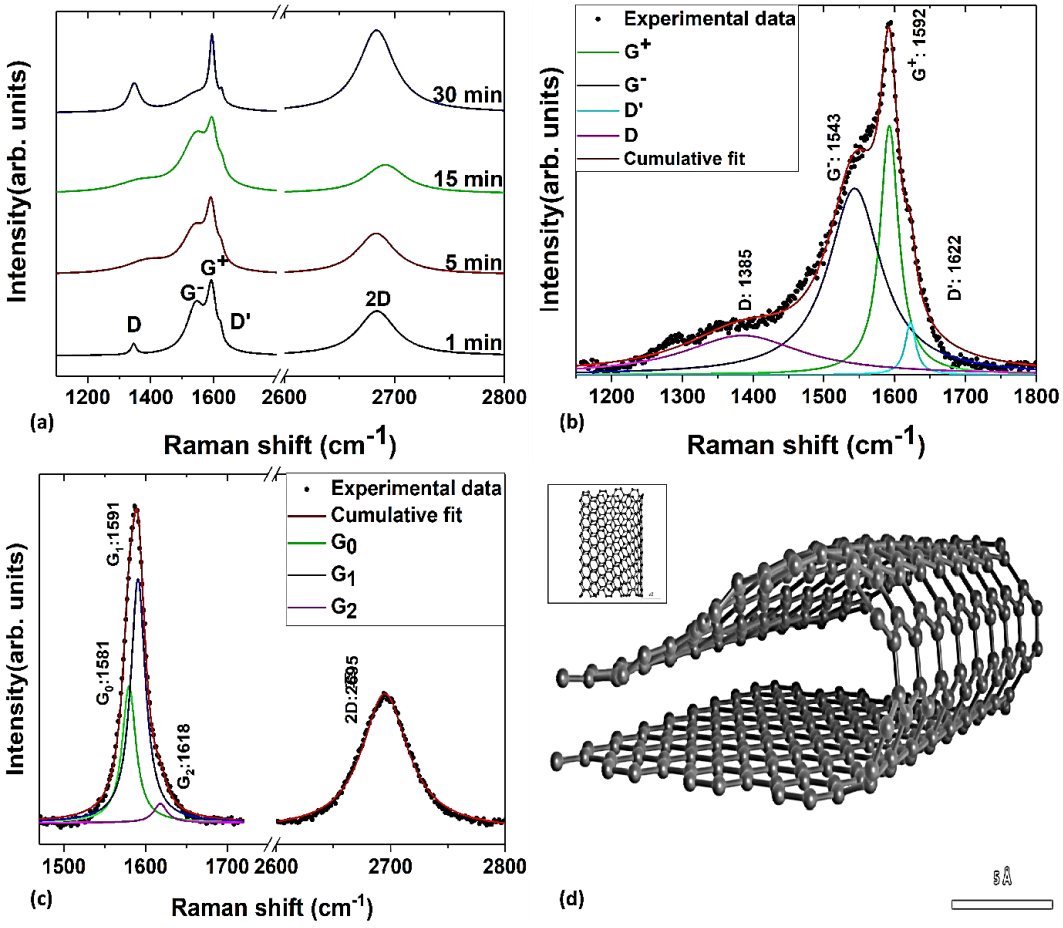

Fig. 3. (a) Raman spectrum of grown graphene with different growth time, 1 min, 5 min, 15 min and 30 min (b) deconvoluted Raman spectrum of graphene sample grown for 5 min showing signature Raman bands of graphene viz: D, G^-, G^+ and D' (c) Raman spectrum of graphene grown for 30 min intercalated with $FeCl_3$ (d) 3-D visualization of folding of graphene, inset show top view (color online)

In Fig. 3(b), two other Raman bands D (~1385 cm^{-1}) and D' (~1622 cm^{-1}) can also be observed. These bands correspond to single phonon intervalley and intervalley scattering events respectively [8]. They appear in the presence of disorders in the otherwise perfect, honey comb structured sp^2 hybridized nano carbon structure. The presence of the two defect bands suggest that the defect in the region probed by Raman spectroscopy are point defects (eg. Resonant scatterers and substitutional atoms) [19].

The distance between defects (L_D) can be construed as a measure of the amount of disorder in the graphene sample. L_D is known to have an inverse relationship with $\frac{I_D}{I_G}$ and it is detailed by the expression [8]:

$$L_D^2 = \frac{4.3\times10^3}{E_L^4} \times \left[\frac{I_D}{I_G}\right]^{-1} (nm^2) \quad (1)$$

where $E_L = \hbar\omega_L\ (eV)$ is the laser excitation energy.

By calculating $\frac{I_D}{I_G}$ ratios from Fig. 3(a) and using the fact that a 532 nm laser was used to record the Raman spectra, distance between point defects are calculated to be approximately 28 nm, 26 nm, 25 nm and 19 nm for graphene samples with growth time 1, 5, 15 and 30 minutes respectively. From the calculated results, it can be inferred that all the synthesized graphene layers are in the first stage of defect evolution [8]. Fig. 3 (c) exhibits the Raman spectrum of CVD graphene grown for 30 minutes intercalated with $FeCl_3$. Intercalation, a process by which atomic or molecular species fill the spaces in a layered structure, with $FeCl_3$ induces a strong charge transfer from graphene to $FeCl_3$, thereby leading to high level of hole doping in the graphene sheets [20]. This hole doping causes a shift in the Fermi energy in graphene layers. Consequently, this leads to a change in the phonon dispersion close to Kohn anomalies (KA) [20], which are nothing but the anomalous behavior of phonon dispersion caused due to rapid changes in the screening of atomic vibrations, associated with certain points of the Brillion zones, by electrons [21]. It has been reported that the G peak's composition and position directly relates to the level of doping [20]. The G peak typically splits into 3 constituent peaks (G_0: 1581, G_1: 1591 and G_2: 1618) as shown in Fig. 3 (c). An area weighted position of the G peak can be calculated using the expression [22]:

$$< PosG > = \frac{PosG_0\frac{AreaG_0}{2} + PosG_1 AreaG_1 + PosG_2 AreaG_2}{\frac{AreaG_0}{2} + AreaG_1 + AreaG_2} \quad (2)$$

$PosG_x$ (cm^{-1}) is the position of the G_x peak and $AreaG_x$ is the area under G_x peak. Using values extracted from Fig. 3(c) $< PosG >$ is calculated to be approximately 1590 cm^{-1}. The 2D band shown in Fig. 3(c) is a single peak that can be fit using a single Lorentzian curve. This indicates electronic decoupling of the FLG and intercalation by $FeCl_3$ [23].

In order to understand the spatial distribution of the Raman features on the synthesized graphene, maps of the Raman features are constructed as described in the experimental section. Because Raman spectroscopic analysis is performed on graphene samples transferred on to SiO_2 substrate, the uniform Raman spectroscopic response of the SiO_2 substrate can be used to understand the graphene layer in a detailed and reliable manner. By using Raman shift of silicon occurring at 520 cm^{-1}, one could arrive at definite conclusions about the stacking order and layer numbers of the synthesized grapheme [10]. By using the stacking determination function developed by Hwang et al. [10]:

$$stacking\left(\frac{A_G}{A_{Si}}, \frac{A_{2D}}{A_G}\right) = \begin{cases} monolayer, if\ 0.03 < \frac{A_G}{A_{Si}} \leq 0.181 \\ AB\ Bernal, if\ \frac{A_G}{A_{Si}} > 0.181\ and\ \frac{A_{2D}}{A_G} < 2.40 \\ turbostatic, if\ \frac{A_G}{A_{Si}} > 0.181\ and\ \frac{A_{2D}}{A_G} > 4.08 \\ unknown, if\ none\ of\ the\ above\ conditions\ hold \end{cases} \quad (3)$$

and the mean values of $\frac{A_G}{A_{Si}}$ and $\frac{A_{2D}}{A_G}$ mentioned in Fig. 4 (b,e,h,k) and Fig. 4 (a,d,g,j) respectively, we can conclude that graphene synthesized with growth times 1, 5, 15 and 30 minutes are multilayered or few layered (FLG) and AB Bernal stacked.

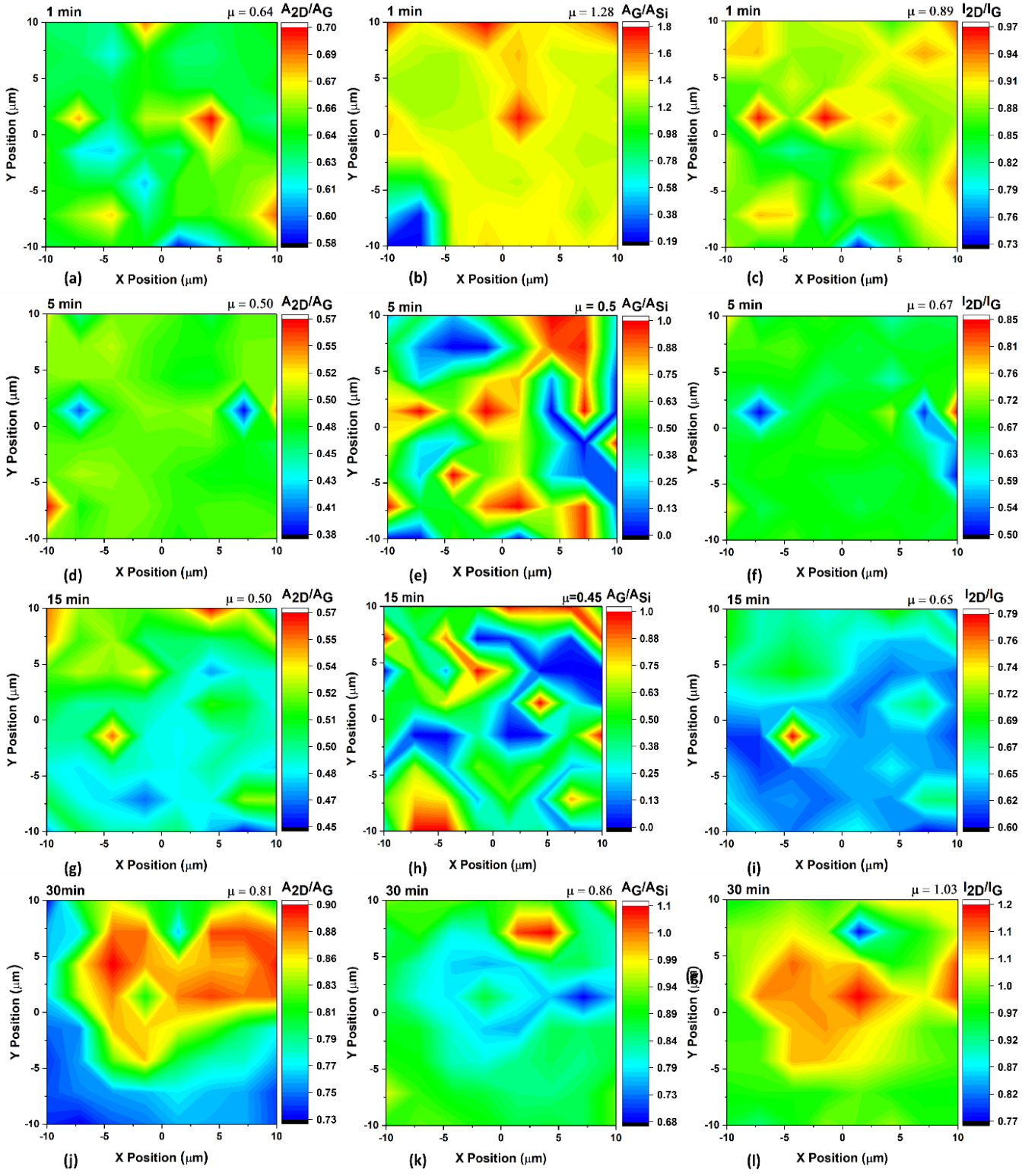

Fig. 4. Mapping of Raman spectroscopy ratios A_{2D}/A_{Si} (a,d,g,j), A_G/A_{Si} (b,e,h,k), I_{2D}/I_G (c,f,i,l) of CVD grown graphene transferred on to SiO_2 substrate with growth time 1 min (a-c), 5 min (d-f), 15 min (g-i) and 30 min (j-l) (color online)

3.3. Elemental analysis using XPS

XPS analysis of graphene quantifies the defects present through the calculation of $\frac{O}{C}$ ratio and different types of carbon bonds present. Fig. 5 shows the C1s spectra of FLG, grown for 30 minutes and transferred on SiO_2. The background of the data is removed using the standard Shirley baseline removal method [24]. The constituent peaks are deconvoluted using Voigt curves. Deconvolution reveals three constituent peaks at

approximate binding energies 285 eV, 286 eV and 289 eV corresponding to sp^2 C=C bond, sp^3 C-C bond and O=C-O (carboxyl) group respectively [25].

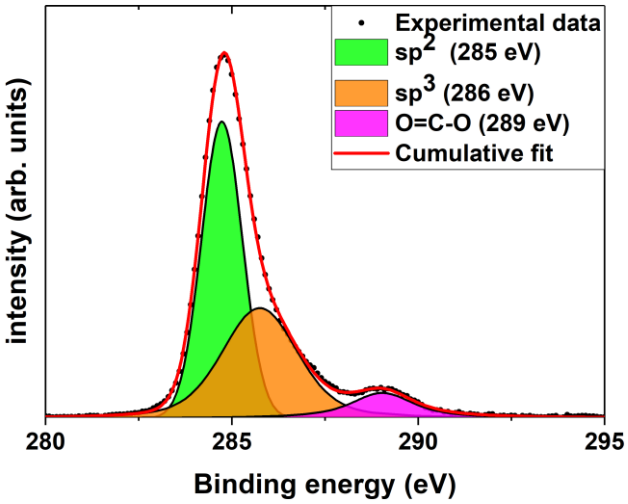

Fig. 5. XPS C1s spectra of CVD graphene grown for 30 minutes (color online)

Curve fitting with the above-mentioned constituent peaks yields a very good fit with R-Squared value of 0.99. Following the deconvolution of the XPS spectrum the $\frac{O}{C}$ ratio can be calculated using the expression [26]:

$$\frac{O}{C}_{fit} = \frac{A_{C-OH}+A_{C=O}+\frac{1}{2}.A_{C-O-C}+2.A_{O=C-O}}{A_{tot}} \quad (4)$$

A_x is the area of a oxygenated group and A_{tot} is the total area under the curve.

From Fig. 5, it can be seen that most of the oxygenated groups are absent except for the carboxyl group (O=C-O) with peak at 289 eV. Using the area under the curves, the $\frac{O}{C}$ ratio is calculated to be 0.18. This indicates moderate oxygen content in the graphene sample. This oxygen content in the FLG is likely to occur due to the transfer procedure used and atmospheric exposure.

4. Conclusion

Few layered graphene was synthesized using CVD. The synthesized graphene layers were characterized using Raman spectroscopy. Detailed study of the Raman spectrum revealed the presence of strain and rolling of graphene layers. Average distance between defects were calculated using $\frac{I_D}{I_G}$. Distribution of Raman features were analyzed using maps of the Raman spectrum of the synthesized graphene layers. Raman ratios obtained from the maps were used to conclude that the synthesized graphene layers were multilayerd and Bernal stacked. Graphene layers were intercalated using $FeCl_3$ and were analyzed using Raman spectroscopy. The analysis revealed splitting of the G band and stiffening of 2D band. FESEM analysis of the synthesized graphene revealed various features such as the underlying copper foil, graphene layers, impurities and folds. Grayscale histogram analysis of the FESEM images revealed a monotonic increase in coverage by graphene over the copper surface as the growth time increased. XPS analysis revealed the presence of sp^2, sp^3 hybridized carbon and the presence of oxygenated carbon groups. The oxygen content was quantified by calculating the $\frac{O}{C}$ ratio from the XPS spectrum.

Acknowledgements

The authors thank UGC-DAE-CSR, Mumbai node for providing financial assistance under the grant UDCSR/MUM/CD/CRS-M-294/2018/146.

References

[1] A. C. Ferrari, F. Bonaccorso, V. Fal'ko, K. S. Novoselov, S. Roche, P. Bøggild, S. Borini, F. H. L. Koppens, V. Palermo, N. Pugno, J. A. Garrido, R. Sordan, A. Bianco, L. Ballerini, M. Prato, E. Lidorikis, J. Kivioja, C. Marinelli, T. Ryhänen, A. Morpurgo, J. N. Coleman, V. Nicolosi, L. Colombo, A. Fert, M. Garcia-Hernandez, A. Bachtold, G. F. Schneider, F. Guinea, C. Dekker, M. Barbone, Z. Sun, C. Galiotis, A. N. Grigorenko, G. Konstantatos, A. Kis, M. Katsnelson, L. Vandersypen, A. Loiseau, V. Morandi, D. Neumaier, E. Treossi, V. Pellegrini, M. Polini, A. Tredicucci, G. M. Williams, B. Hee Hong, J.-H. Ahn, J. Min Kim, H. Zirath, B. J. van Wees, H. van der Zant, L. Occhipinti, A. Di Matteo, I. A. Kinloch, T. Seyller, E. Quesnel, X. Feng, K. Teo, N. Rupesinghe, P. Hakonen, S. R. T. Neil, Q. Tannock, T. Löfwander, J. Kinaret, Nanoscale **7**, 4598 (2015).

[2] K. S. Novoselov, Science **306**, 666 (2004).

[3] C. N. R. Rao, U. Maitra, H. S. S. R. Matte, Graphene: Synthesis, Properties, and Phenomena, Wiley-VCH Verlag GmbH & Co. KGaA, 2012, pp. 1–47.

[4] L. Álvarez-Fraga, J. Rubio-Zuazo, F. Jiménez-Villacorta, E. Climent-Pascual, R. Ramírez-Jiménez, C. Prieto, A. de Andrés, Chem. Mater. **29**, 3257 (2017).

[5] L. Huang, D. Zhang, F.-H. Zhang, Z.-H. Feng, Y.-D. Huang, Y. Gan, Small **14**, 1704190 (2018).

[6] A. C. Ferrari, J. C. Meyer, V. Scardaci, C. Casiraghi, M. Lazzeri, F. Mauri, S. Piscanec, D. Jiang, K. S. Novoselov, S. Roth, A. K. Geim, Phys. Rev. Lett. **97**, 187401 (2006).

[7] A. C. Ferrari, Solid State Communications **143**, 47 (2007).

[8] A. C. Ferrari, D. M. Basko, Nature Nanotech **8**, 235 (2013).

[9] M. S. Dresselhaus, A. Jorio, A. G. Souza Filho, R.

Saito, Proc. R. Soc. A **368**, 5355 (2010).
[10] J.-S. Hwang, Y.-H. Lin, J.-Y. Hwang, R. Chang, S. Chattopadhyay, C.-J. Chen, P. Chen, H.-P. Chiang, T.-R. Tsai, L.-C. Chen, K.-H. Chen, Nanotechnology **24**, 015702 (2013).
[11] R. Blume, D. Rosenthal, J.-P. Tessonnier, H. Li, A. Knop-Gericke, R. Schlögl, ChemCatChem **7**, 2871 (2015).
[12] I. Khrapach, F. Withers, T. H. Bointon, D. K. Polyushkin, W. L. Barnes, S. Russo, M. F. Craciun, Adv. Mater. **24**, 2844 (2012).
[13] K. C. Kwon, K. S. Choi, S. Y. Kim, Adv. Funct. Mater. **22**, 4724 (2012).
[14] F. Yang, Y. Liu, W. Wu, W. Chen, L. Gao, J. Sun, Nanotechnology **23**, 475705 (2012).
[15] S. M. Kim, A. Hsu, Y.-H. Lee, M. Dresselhaus, T. Palacios, K. K. Kim, J. Kong, Nanotechnology **24**, 365602 (2013).
[16] B. Tang, H. Guoxin, H. Gao, Applied Spectroscopy Reviews **45**, 369 (2010).
[17] T. M. G. Mohiuddin, A. Lombardo, R. R. Nair, A. Bonetti, G. Savini, R. Jalil, N. Bonini, D. M. Basko, C. Galiotis, N. Marzari, K. S. Novoselov, A. K. Geim, A. C. Ferrari, Phys. Rev. B **79**, 205433 (2009).
[18] H. Li, M. Li, Z. Kang, Nanotechnology **29**, 245604 (2018).
[19] L. G. Cançado, A. Jorio, E. H. M. Ferreira, F. Stavale, C. A. Achete, R. B. Capaz, M. V. O. Moutinho, A. Lombardo, T. S. Kulmala, A. C. Ferrari, Nano Lett. **11**, 3190 (2011).
[20] T. H. Bointon, G. F. Jones, A. De Sanctis, R. Hill-Pearce, M. F. Craciun, S. Russo, Sci Rep **5**, 16464 (2015).
[21] I. Milošević, N. Kepčija, E. Dobardžić, M. Damnjanović, M. Mohr, J. Maultzsch, C. Thomsen, Materials Science and Engineering: B **176**, 510 (2011).
[22] S. Lee, K. Lee, Z. Zhong, Nano Lett. **10**, 4702 (2010).
[23] W. Zhao, P. H. Tan, J. Liu, A. C. Ferrari, J. Am. Chem. Soc. **133**, 5941 (2011).
[24] M. Repoux, Surf. Interface Anal. **18**, 567 (1992).
[25] M. Koinuma, H. Tateishi, K. Hatakeyama, S. Miyamoto, C. Ogata, A. Funatsu, T. Taniguchi, Y. Matsumoto, Chem. Lett. **42**, 924 (2013).
[26] A. Kovtun, D. Jones, S. Dell'Elce, E. Treossi, A. Liscio, V. Palermo, Carbon **143**, 268 (2019).

*Corresponding author: balajic@ssn.edu.in